

The weak electronic correlations and absence of heavy Fermion state in KNi_2Se_2

Q. Fan,^{1,2} X. P. Shen,^{1,2} M. Y. Li,³ D. W. Shen,^{3,*} W. Li,³ X. M. Xie,³ Q. Q. Ge,^{1,2} Z. R. Ye,^{1,2} S. Y. Tan,^{1,2} X. H. Niu,^{1,2} B. P. Xie,^{1,2} and D. L. Feng^{1,2,†}

¹*State Key Laboratory of Surface Physics, Department of Physics, and Advanced Materials Laboratory, Fudan University, Shanghai 200433, P. R. China*

²*Collaborative Innovation Center of Advanced Microstructures, Nanjing 210093, P. R. China*

³*State Key Laboratory of Functional Materials for Informatics, Shanghai Institute of Microsystem and Information Technology (SIMIT), Chinese Academy of Sciences, Shanghai 200050, P. R. China*

(Dated: October 21, 2018)

We have studied the low-lying electronic structure of a new ThCr_2Si_2 -type superconductor KNi_2Se_2 with angle-resolved photoemission spectroscopy. Three bands intersect the Fermi level, forming complicated Fermi surface topology, which is sharply different from its isostructural superconductor $\text{K}_x\text{Fe}_{2-y}\text{Se}_2$. The Fermi surface shows weak variation along the k_z direction, indicating its quasi-two-dimensional nature. Further comparison with the density functional theory calculations demonstrates that there exist relatively weak correlations and substantial hybridization of the Ni $3d$ and the Se $4p$ orbitals in the low-lying electronic structure. Our results indicate that the large density of states at the Fermi energy leads to the reported mass enhancement based on the specific heat measurements. Moreover, no anomaly is observed in the spectra when entering the fluctuating charge density wave state reported earlier.

PACS numbers: 74.25.Jb, 74.70.-b, 79.60.-i, 71.20.-b

I. INTRODUCTION

The iron-chalcogenide superconductors $\text{A}_x\text{Fe}_{2-y}\text{Se}_2$ ($\text{A}=\text{K}, \text{Rb}, \text{etc.}$) with superconducting transition temperature (T_c) up to 33 K have aroused a great deal of research interests¹⁻⁷. Compared with the iron pnictide superconductors, $\text{A}_x\text{Fe}_{2-y}\text{Se}_2$ exhibits some unique properties, such as the antiferromagnetically ordered insulator parent compound with Fe vacancy order³⁻⁶. Particularly, angle-resolved photoemission spectroscopy (ARPES) revealed that the Fermi surface of the superconducting phase is consisted of electron pockets only, raising a serious challenge to the prevalent Fermi surface nesting mechanism for the superconductivity in iron-based superconductors^{8,9}.

Recently, another chalcogenide superconductor KNi_2Se_2 was reported¹⁰, which shares the same crystal structure and almost the same lattice constants with $\text{K}_x\text{Fe}_{2-y}\text{Se}_2$, except that there are no vacancies in KNi_2Se_2 ¹¹. However, previous experiments indicated that KNi_2Se_2 displays a rich but sharply different phase diagram from that of $\text{K}_x\text{Fe}_{2-y}\text{Se}_2$. Based on the specific heat measurements and neutron pair-distribution-function analysis, KNi_2Se_2 was suggested to show a local charge density wave (CDW) fluctuating state above 20 K, which then enters a coherent heavy-Fermion state at lower temperatures. Eventually, it becomes superconducting below ~ 0.8 K¹⁰. The large linear specific heat coefficient (or Sommerfeld coefficient, γ) was proposed to be due to the strong electron correlation and heavy Fermion behavior in KNi_2Se_2 . More specifically, mix valency of the Ni atoms was proposed to induce the heavy effective band mass m^* . On the other hand, we note that the band renormalization factor of BaNi_2As_2

(a superconductor with $T_c \sim 0.7$ K) is merely ~ 1.66 , in the weak-interaction regime, and thus the conventional electron-phonon interaction mechanism was suggested to be the cause of the superconductivity therein¹². In an ionic picture, the Ni orbital configuration is $3d^8$ for BaNi_2As_2 , and $3d^{8.5}$ for KNi_2Se_2 . Consequently, the Hund's rule coupling and electron correlations should be weakened with the increasing number of $3d$ electrons in the latter compound¹³, which is inconsistent with the proposed heavy Fermion scenario in KNi_2Se_2 . To resolve this controversy and understand the unique properties of KNi_2Se_2 , it is critical to study its electronic structure.

In this article, we have systematically studied the electronic structure of the single-crystalline KNi_2Se_2 with ARPES. There are two electron pockets around the M point, a hole-like square pocket surrounding the Γ point, and a hole-like narrow race-track pocket surrounding the X point, respectively. The electronic structure of KNi_2Se_2 shows relatively weak k_z dependence, indicative of its two-dimensional (2D) character. Further comparison between the density functional theory (DFT) band calculations and ARPES data gives a renormalization factor of about 1.54, which indicates that the electron correlations are weak. The coherent bands are present at high temperatures, and there is no incoherent-weight-to-coherent-band transition at low temperatures as in heavy Fermion materials. Instead, we find that the Fermi velocities of several bands are relatively small and thus enhance the density of states (DOS) at the Fermi energy (E_F). Our quantitative analysis shows that the large γ of KNi_2Se_2 together with those of BaNi_2As_2 and KFe_2As_2 (which has even larger γ), can be well accounted by the multiple large Fermi surfaces and relatively small Fermi velocities in these systems without invoking any heavy

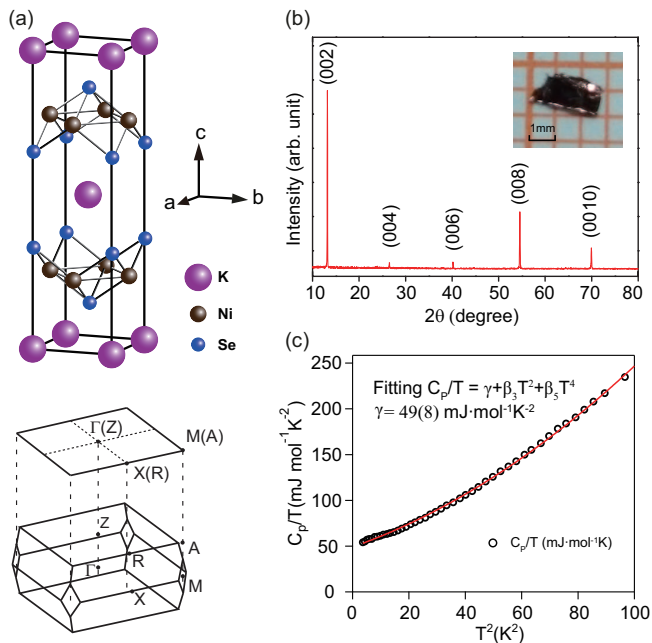


FIG. 1: (Color online) (a) Representative unit cell of KNi₂Se₂ (upper panel) and its Brillouin zone (lower panel). Note one tetragonal unit cell of KNi₂Se₂ contains two chemical formula units. For the convenience, the 2D Brillouin zone is referred hereafter, which is the projection of the three-dimensional Brillouin zone. (b) X-ray diffraction patterns of KNi₂Se₂ single crystal after cleavage. The inset shows the photo of a typical single crystal. (c) The low-temperature specific heat data of KNi₂Se₂ divided by temperature versus temperature squared, revealing a large linear electronic contribution to the low-temperature heat capacity.

Fermion physics.

II. EXPERIMENTAL

High quality single crystals of KNi₂Se₂ were grown by self-flux method with nominal composition K:Ni:Se = 1:2:2. The mixture was loaded into the alumina crucible and then sealed in an argon-filled iron crucible. The entire assembly was kept at 1273 K for 3 hours, and then cooled down to 873 K slowly at a rate of ~ 4 K/h before shutting off the power. The samples are crystallized in the tetragonal ThCr₂Si₂-type structure with the space group $I4/mmm$, as shown in Fig. 1(a)¹⁴. The as-grown single crystals with a typical dimension of $2.5 \times 1.0 \times 0.1$ mm³ show flat shiny surface of pink color after cleavage [the inset of Fig. 1(b)]. The electron probe micro analysis (EPMA) measurements across samples with more than 10 points indicate that the composition is quite homogeneous, and the averaged stoichiometric ratio is determined to be KNi_{2.06}Se_{2.01}. Since this determined composition is close to the stoichiometry, we will still designate the samples as KNi₂Se₂ for convenience hereafter. In Fig. 1(b), X-ray diffraction measurements

show that only the series of (00 l) narrow reflection peaks appear, suggestive of the good crystalline quality. The low-temperature specific heat [Fig. 1(c)] can be well fitted by the formula $C_p/T = \gamma + \beta_3 T^2 + \beta_5 T^4$ in the temperature range from 1.8 K to 10 K, and the resulting large Sommerfeld coefficient [$\gamma = 49.8$ mJ mol⁻¹ K⁻²] is in good agreement with previous reports^{10,11}. For comparison, we note that the corresponding γ is about 13.2 mJ mol⁻¹ K⁻² for BaNi₂As₂¹⁵, and about 94.3 mJ mol⁻¹ K⁻² for KFe₂As₂¹⁷.

ARPES measurements were performed at (1) Beamline 7U of the UVSOR synchrotron facility with a MBS A-1 electron analyzer, (2) Beamline 28A of Photon Factory (PF), KEK, Tsukuba, with a Scienta SES-2002 analyzer, and (3) the in-house system equipped with an SPECS UVLS helium discharging lamp and VG Scienta R4000 electron analyzer. The overall energy resolution was set to 15-30 meV depending on the photon energy, and the typical angular resolution was 0.3°. Samples were cleaved *in situ* and then measured under ultrahigh vacuum better than 6×10^{-11} mbar. The sample surfaces were stable and did not show any sign of degradation during the measurements.

The first-principles calculations were implemented in the VASP code¹⁸. The plane wave basis method and the Perdew-Burke-Ernzerhof¹⁹ exchange correlation potential have been used. Throughout the calculations, a 500 eV cutoff in the plane wave expansion and a $12 \times 12 \times 12$ Monkhorst-Pack \vec{k} grid were chosen to ensure the calculation with an accuracy of 10^{-5} eV. In our calculations, the crystal structure and lattice constants were taken from the experimental values^{10,14}.

III. EXPERIMENTAL RESULTS

The photoemission intensity map of KNi₂Se₂ at 15 K is shown in Fig. 2(a), which is overlaid on the projected 2D Brillouin zone. The resulting Fermi surface (FS) consists of one square-like Fermi pocket around the zone center, two Fermi pockets around zone corner, and one narrow race-track pocket extending to the middle of zone boundaries, as highlighted by the colored dashed lines. This complicated FS is a direct evidence of the multi-band behavior in this compound, consistent with previous Hall effect measurement¹¹ and theoretical calculations^{20,21}. Although this multi-band character is similar to iron-based superconductors, the detailed FS topology of KNi₂Se₂ is distinct from that of K_xFe_{2- y} Se₂, which only exhibits circular electron-like pockets around the zone corner^{8,9}.

Now we examine the band dispersions of KNi₂Se₂ along several high-symmetry directions as indicated in the lower panel of Fig. 2(a). We chose 75 eV photons to probe the band structure near the Γ XM plane of KNi₂Se₂ considering an inner potential of 15 eV as discussed below. Along Γ - M [cut #1 in Fig. 2(b)], three Fermi crossings can be identified by fitting the corresponding momentum distribution curve (MDC) at E_F . More-

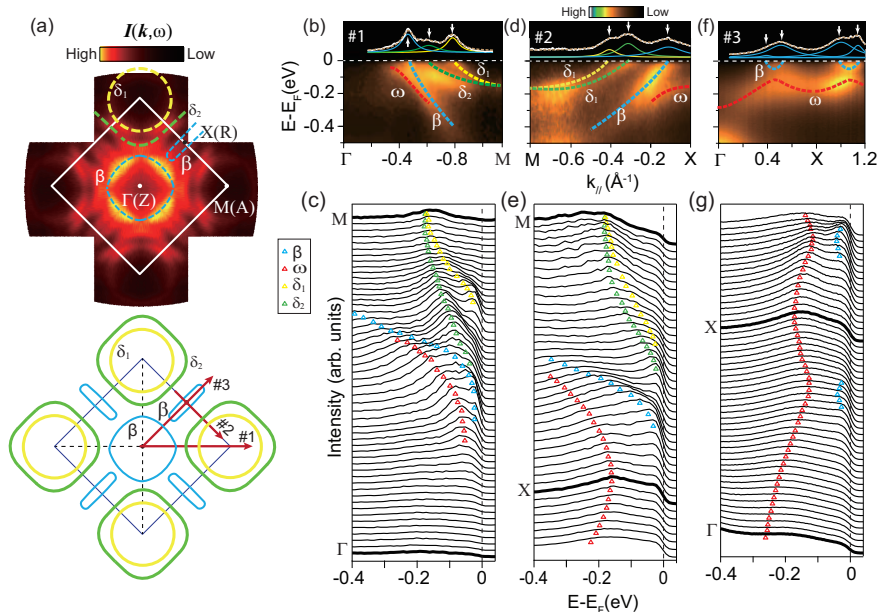


FIG. 2: (Color online) Electronic structure of KNi_2Se_2 measured at 15 K. (a) Photoemission intensity map integrated over $[E_F - 10 \text{ meV}, E_F + 10 \text{ meV}]$ (upper panel) and the 2D projected Brillouin zone of KNi_2Se_2 (lower panel). It was obtained through mirroring the data with respect to both k_x and k_y axes. (b) The photoemission intensity along cut #1 ($\Gamma - M$ direction). (c) Selected EDCs for data in (b). (d) and (e), (f) and (g) show the similar data as in (b) and (c), but along cut #2 and cut #3, respectively. The data in panel (a) were taken with randomly polarized 21.2 eV photons from a helium discharge lamp, and the other data were taken with circularly polarized 75 eV photons at KEK.

over, the corresponding band dispersions can be tracked with the peaks in the energy distribution curves (EDCs) [Fig. 2(c)], and they are assigned as β , δ_1 , and δ_2 , respectively. Among them, the hole-like β band encloses the Γ point, forming the square-shaped Fermi pocket; while, the δ_1 and δ_2 bands seem to be degenerate at the M point with the band bottoms at 180 meV, developing two electron pockets around the zone corner. Besides, there is another weak feature (ω) around the Γ point, whose band top is about 50 meV below E_F . Along $M - X$ [cut #2 in Fig. 2(d)], three bands cross E_F as well, which are further confirmed by the peaks in the corresponding MDC fitting and EDCs [Fig. 2(e)]. Taking into account the bottom positions of these bands, we can infer that these two electron-like bands around M are the δ_1 and δ_2 bands, respectively. Based on the band calculations presented in Fig. 4 later, the band near X (marked by blue dashed lines) is β .

Along $\Gamma - X$, data in Figs. 2(f) and 2(g) show a shallow electron-like band (blue dashed line). Based on the analysis presented in Fig. 4 later, this feature is actually contributed mostly by the β band. Such a shallow electron-like band is due to a pronounced hybridization between β and ω shown here. However, it does not develop into a closed electron pocket. Instead, it forms the narrow race-track hole-like Fermi pocket (β) surrounding X .

To fully reveal the Fermi surface topology in the three-dimensional Brillouin zone, we have performed detailed photon energy dependent ARPES measurements. Along cut #1, only β band shows up in the s polarization [Fig. 3(a)]. The Fermi momenta (k_F 's) of β are determined by peak positions in MDCs in [Fig. 3(d)]. Taking the inner potential of 15 eV to estimate the k_z 's for different photon energies, we notice that k_F 's of β move periodically from Γ (probed with 21 eV photons) to Z

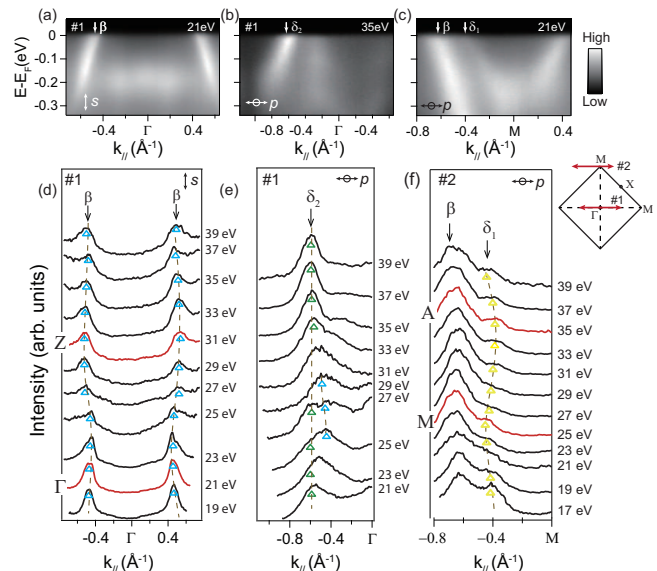


FIG. 3: (Color online) (a) The photoemission intensity taken along cut #1 with s polarized 21 eV photons. (b) The photoemission intensity taken along cut #1 with p polarized 35 eV photons. (c) is the same as (a) but along cut #2. (d) and (e) are MDCs at E_F taken with different photon energies along cut #1 in s and p polarizations, respectively. (f) is the same as (d) but taken along cut #2 in p polarization. Data were taken at Beamline 7U of UVSOR, and the temperature was 66 K.

(probed with 31 eV photons). Our data could cover more than half of the Brillouin zone along the k_z direction. On the other hand, δ_2 is clearly resolved in the p polarization [Fig. 3(b)], which shows negligible k_z dispersion as shown in Fig. 3(e). Along cut #2, β and δ_1 band show up in the p polarization [Fig. 3(c)]. As shown in Fig. 3(f), there is

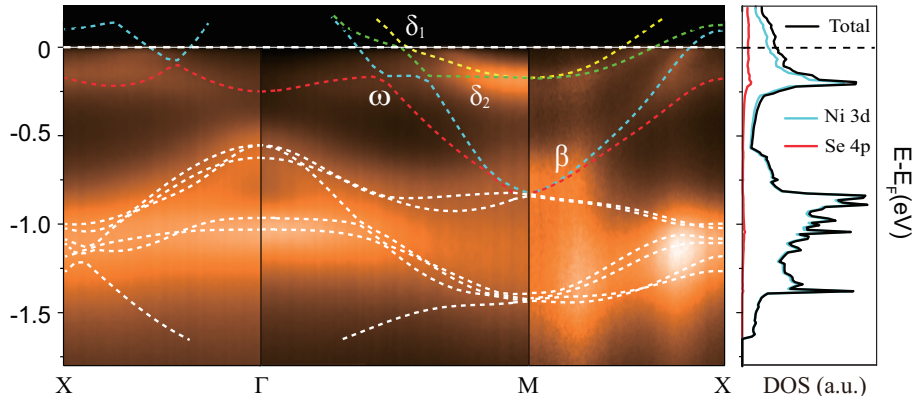


FIG. 4: (Color online) (Left) Comparison of the ARPES experimental band structure and the DFT calculation results along the high symmetry directions in KNi_2Se_2 . (Right) Calculated density of states of KNi_2Se_2 . Blue and red curves correspond to Ni and Se partial DOS, respectively.

some dispersion along k_z for the δ_1 band. In general, the k_z dispersions of these bands are not strong, manifesting the 2D nature of KNi_2Se_2 . Our result is consistent with the previous theoretical calculations except for the hole-like pocket centered at the Γ point, which was suggested to be more three-dimensional-like^{20,21}. This discrepancy might be partially attributed to the poor k_z resolution in ARPES experiments.

IV. DISCUSSIONS AND CONCLUSIONS

The measured quasi-2D electronic structure of KNi_2Se_2 is compared with the band structure obtained from our first-principles calculations. In Fig. 4, the calculated band (dashed lines) are scaled and appended onto the photoemission intensity plots along the three high symmetry directions. Here, a renormalization factor of about 1.54 to the calculations leads to a remarkable agreement with the experimental data. Almost all characteristic dispersions, even the small electron-like feature along $\Gamma - X$ direction, can be reproduced well by the calculations. This relatively small renormalization factor demonstrates that the electron correlations in this system are rather weak. Furthermore, we present the calculated total DOS and the projected DOS of KNi_2Se_2 in the right panel of Fig. 4. Near E_F , there are some contribution from the Se 4p orbitals in addition to the dominating contribution from Ni 3d orbitals.

The small renormalization factor found here for KNi_2Se_2 is similar to that of BaNi_2As_2 (~ 1.66)¹², which suggests that electron correlations are weak in both systems. This is consistent with their Ni orbital configurations, *i.e.* $3d^8$ for BaNi_2As_2 , and $3d^{8.5}$ for KNi_2Se_2 . Hund's rule coupling is the main source of correlations

in these materials, and it has been shown recently that the correlations are reduced dramatically from $3d^6$ to $3d^7$ with electron doping, and superconductivity diminishes with weakened correlations¹³. Therefore, compared with the iron-based superconductors, the even higher 3d occupation and weaker correlations in these Ni-based compound suggest that the superconductivity is most likely due to the electron-phonon coupling, similar to that in the multi-band superconductor MgB_2 ^{26,27}.

One of the most intriguing aspects of KNi_2Se_2 is the possible heavy electronic state existing below ~ 20 K (T_H), with an enhanced effective electronic band mass. However, this is not consistent with the well-defined bands observed at 15 K and the weakly correlated electronic structure. To understand the origin of the large Sommerfeld coefficient in KNi_2Se_2 , we compare its specific heat and electronic structure with those of BaNi_2As_2 and KFe_2As_2 . The latter has a Fe $3d^{5.5}$ orbital configuration, which fosters stronger Hund's rule coupling and higher electron correlations (renormalization factor $2 \sim 4$)¹⁶, leading to higher γ ($94.3 \text{ mJ mol}^{-1} \text{ K}^{-2}$)¹⁷. Meanwhile, the γ is $49.8 \text{ mJ mol}^{-1} \text{ K}^{-2}$ for of KNi_2Se_2 , and $13.2 \text{ mJ mol}^{-1} \text{ K}^{-2}$ for BaNi_2As_2 ¹⁵.

As the electronic specific heat γ coefficient is proportional to the DOS at E_F , which can be further estimated by the formula $\gamma \propto \sum_n \int_{s_n(E_F)} \frac{ds}{|\nabla_k E(k_F)|}$, where n is the band index, $|\nabla_k E(k_F)|$ is the mean velocity of an electron at E_F . For a 2D system, the formula can be simplified through: $ds \rightarrow$ the perimeter of Fermi surface, and $|\nabla_k E(k_F)| \rightarrow$ the Fermi velocity or the band slope at E_F . Thus we can roughly evaluate the DOS at E_F of these systems, as shown in Fig. 5.

By estimation, we notice that the total Fermi surface perimeters are similar for all three systems [Figs. 5(a),

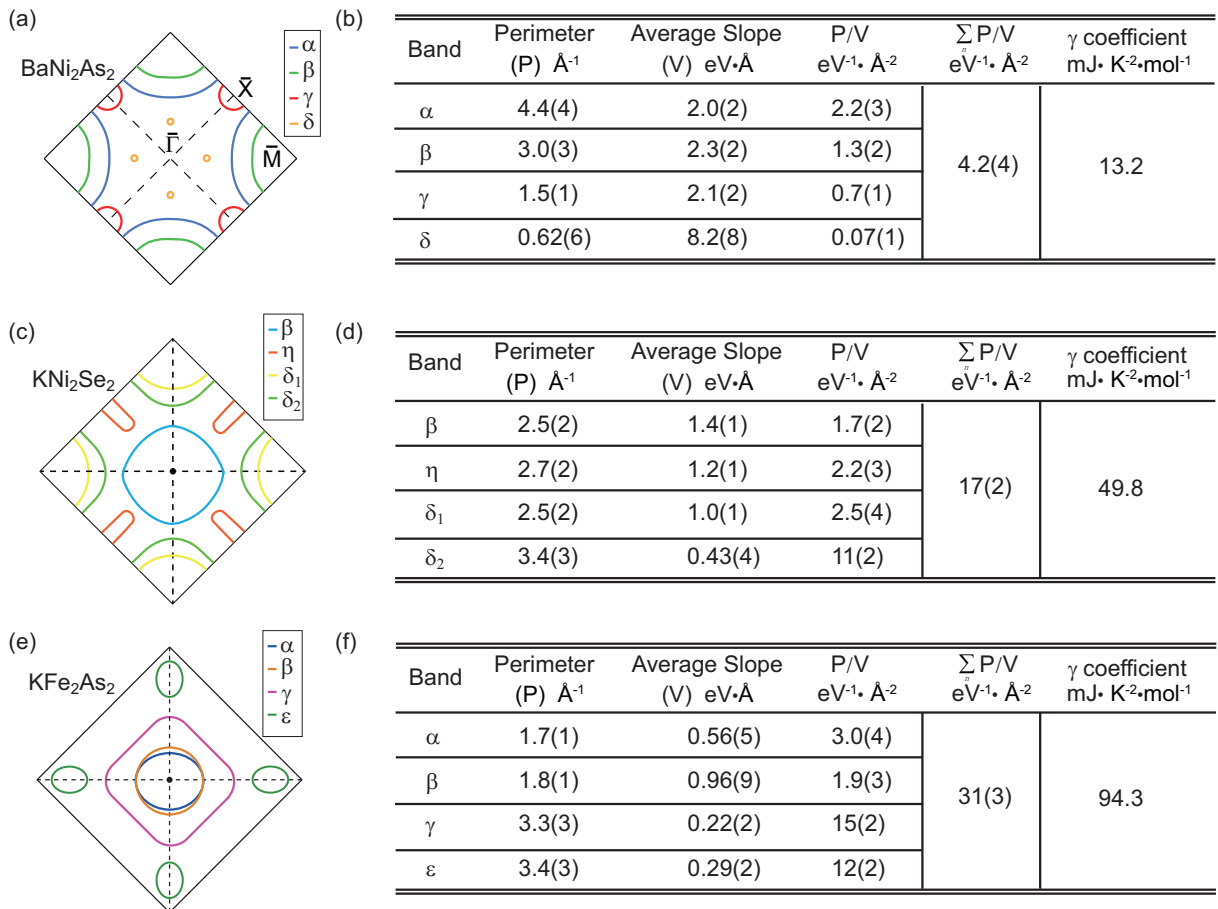


FIG. 5: (Color online) (a) Sketch of Fermi surface for BaNi_2As_2 , reproduced from Ref.¹². (b) The DOS estimation of each band in BaNi_2As_2 system. (c) and (d), (e) and (f) are the same as in panels (a) and (b), but for KNi_2Se_2 and KFe_2As_2 , respectively.

5(c), and 5(e)]. However, the average Fermi velocity decreases rapidly in the order of BaNi_2As_2 , KNi_2Se_2 and KFe_2As_2 [Figs. 5(b), 5(d), and 5(f)]. Consequently, the estimated DOS value in KNi_2Se_2 is 4.0(6) times of that of BaNi_2As_2 , which is generally consistent with the corresponding ratio (3.8) of their γ coefficients. Similarly, both the estimated DOS and γ of KFe_2As_2 are about 1.8~1.9 times of those of KNi_2Se_2 . Therefore, our data suggest that the large γ in KNi_2Se_2 is due to the relatively flat bands (especially δ_2) in combination with the large Fermi surface perimeters, instead of the heavy Fermion state. These are confirmed by our DFT calculations, which gives flat δ_1 and δ_2 . Our results also suggest that the large γ in KFe_2As_2 is not due to heavy Fermion physics, but due to strong correlations or Hund's rule coupling there as well. Furthermore, the remarkably good agreement between the estimated DOS at E_F and the measured γ for all three systems with different levels of correlation strength shows that this new way of quantitative analysis can provide valuable insight for understanding the thermal dynamical properties of these multi-band materials.

The neutron pair-distribution-function analysis revealed that the local CDW fluctuation occurs at T_H and

disappears upon further cooling¹. Temperature evolution of the electronic structure is shown in Fig. 6. The photoemission intensity along $\Gamma - M$ (cut #1) was displayed in Fig. 6(b), we found that there is no evident spectral weight change with temperature within our energy resolution, except for some thermal broadening effects [Fig. 6(d)]. Along $M - X$ (cut #2), as shown in Fig. 6(c), there is a spectral weight suppression with increasing temperature for δ_1 , δ_2 , and ω , as indicated by the up arrows in Fig. 6(e). However, the spectral weight suppression rate do not alter noticeably across T_H . Similar spectral weight change was observed in $\text{Sr}_2\text{CuO}_2\text{Cl}_2$ and $\text{BaTi}_2\text{As}_2\text{O}$, which is explained by strong coupling between electrons and magnons or phonons^{23,24}. For $\text{BaTi}_2\text{As}_2\text{O}$, a change of the spectral weight evolution rate was observed at the CDW ordering temperature. The absence of anomaly at T_H here is likely due to the fact that the CDW fluctuation in KNi_2Se_2 was reported to be dynamic and/or entirely uncorrelated between unit cells within the ab plane, in contrast to the coherent CDWs observed in structurally related compounds such as NbSe_2 ²⁵. Nevertheless, since we observed spectral weight suppression at nested Fermi surface sections, it may indicate that the enhanced electron-phonon interactions

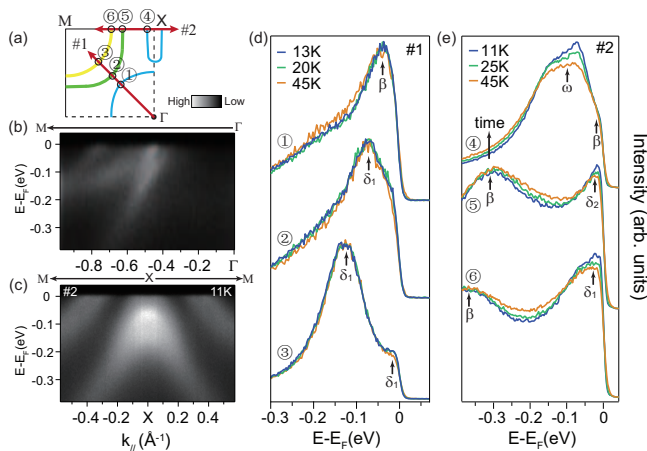


FIG. 6: (Color online) (a) The sketch of a Brillouin zone quadrant. (b) and (c) Photoemission intensities along cuts #1 and #2 as indicated in panel (a), respectively. (d) and (e) Temperature dependence of EDCs at various momenta as marked in panel (a). The data in panels (b) and (d) were taken with circularly polarized 75 eV photons at KEK, and the other data were taken with randomly polarized 21.2 eV photons from a helium discharge lamp.

in these sectors may be responsible for the local CDW fluctuations.

To summarize, we have systematically studied the electronic structure of KNi_2Se_2 by high-resolution ARPES. There are three bands intersecting the Fermi level, which form two electron-like pockets, one square-like and one elongated elliptical hole-like pockets surrounding the M , Γ and X points, respectively. Furthermore, the

electronic structure of this multi-orbital superconductor shows relatively weak k_z dependence, indicative of its 2D nature. Further comparison with the DFT band calculations suggests that the electron correlations therein are relatively weak. Our results clearly indicate that it is not the heavy Fermion behavior advocated before, but the relative small Fermi velocities of bands in combination with large Fermi surfaces that lead to the large DOS and electronic specific heat coefficient in KNi_2Se_2 . We also practiced a new way to quantitatively estimate DOS from ARPES data, which would provide valuable insight for understanding the thermal dynamic properties. Moreover, we observed intriguing temperature dependence of the electronic structure in the nested Fermi surface sectors, although we did not observe evident anomaly across T_H . This may be consistent with the local fluctuating CDW in KNi_2Se_2 .

V. ACKNOWLEDGEMENT

We gratefully acknowledge the helpful discussions with Prof. Xiangang Wan. This work was supported by National Basic Research Program of China (973 Program) under the grant Nos. 2011CBA00106, 2011CBA00112, 2012CB927401, and the National Science Foundation of China under Grant Nos. 11104304, 11227902 and 11274332. M. Y. Li and D. W. Shen are also supported by the ‘‘Strategic Priority Research Program (B)’’ of the Chinese Academy of Sciences (Grant No. XDB04040300).

* Electronic address: dwshen@mail.sim.ac.cn

† Electronic address: dlifeng@fudan.edu.cn

¹ J. G. Guo, S. F. Jin, G. Wang, S. C. Wang, K. X. Zhu, T. T. Zhou, M. He, and X. L. Chen, Phys. Rev. B **82**, 180520 (R) (2010).

² H. D. Wang, C. H. Dong, Z. J. Li, S. S. Zhu, Q. H. Mao, C. M. Feng, H. Q. Yuan and M. H. Fang, Europhys. Lett. **93**, 47004 (2011).

³ M. H. Fang, H. D. Wang, C. H. Dong, Z. J. Li, C. M. Feng, J. Chen, and H. Q. Yuan, Europhys. Lett. **94**, 27009 (2011).

⁴ W. Bao, Q. Huang, G. F. Chen, M. A. Green, D. M. Wang, J. B. He, X. Q. Wang, and Y. Qiu, Chin. Phys. Lett. **28**, 086104 (2011).

⁵ F. Ye, S. Chi, W. Bao, X. F. Wang, J. J. Ying, X. H. Chen, H. D. Wang, C. H. Dong and M. H. Fang, Phys. Rev. Lett. **107**, 137003 (2011).

⁶ Y. J. Yan, M. Zhang, A. F. Wang, J. J. Ying, Z. Y. Li, W. Qin, X. G. Luo, J. Q. Li, J. P. Hu, and X. H. Chen, Scientific Reports, **2**, 212 (2012).

⁷ H. H. Wen, Rep. Prog. Phys. **75**, 112501 (2012).

⁸ T. Qian, X. P. Wang, W. C. Jin, P. Zhang, P. Richard, G. Xu, X. Dai, Z. Fang, J. G. Guo, X. L. Chen, and H. Ding,

Phys. Rev. Lett. **106**, 187001 (2011).

⁹ Y. Zhang, L. X. Yang, M. Xu, Z. R. Ye, F. Chen, C. He, H. C. Xu, J. Jiang, B. P. Xie, J. J. Ying, X. F. Wang, X. H. Chen, J. P. Hu, M. Matsunami, S. Kimura, and D. L. Feng, Nat. Mater. **10**, 273 (2011).

¹⁰ J. R. Neilson, A. Llobet, A. V. Stier, L. Wu, J. J. Wen, J. Tao, Y. M. Zhu, Z. B. Tesanovic, N. P. Armitage, and T. M. McQueen, Phys. Rev. B **86**, 054512 (2012).

¹¹ H. C. Lei, M. Abeykoon, K. F. Wang, E. S. Bozin, H. Ryu, D. Graf, J. B. Warren, and C. Petrovic, J. Phys.: Condens. Matter. **26**, 015701 (2014).

¹² B. Zhou, M. Xu, Y. Zhang, G. Xu, C. He, L. X. Yang, F. Chen, B. P. Xie, X. Y. Cui, M. Arita, K. Shimada, H. Namatame, M. Taniguchi, X. Dai, and D. L. Feng, Phys. Rev. B **83**, 035110 (2011).

¹³ Z. R. Ye, Y. Zhang, F. Chen, M. Xu, J. Jiang, X. H. Niu, C. H. P. Wen, L. Y. Xing, X. C. Wang, C. Q. Jin, B. P. Xie, and D. L. Feng, Phys. Rev. X **4**, 031041 (2014).

¹⁴ J. R. Neilson and T. M. McQueen, J. Am. Chem. Soc. **134**, 7750 (2012).

¹⁵ A. S. Sefat, M. A. McGuire, R. Y. Jin, B. C. Sales, D. Mandrus, F. Ronning, E. D. Bauer, and Y. Mozharivskyj, Phys. Rev. B **79**, 094508 (2009).

- ¹⁶ T. Sato, K. Nakayama, Y. Sekiba, P. Richard, Y.-M. Xu, S. Souma, T. Takahashi, G. F. Chen, J. L. Luo, N. L. Wang, and H. Ding, *Phys. Rev. Lett.* **103**, 047002 (2009).
- ¹⁷ M. A. Hafeez, S. Aswartham, S. Wurmehl, V. Grinenko, C. Hess, S. L. Drechsler, S. Johnston, A. U. B. Wolter, B. Büchner, H. Rosner, and L. Boeri, *Phys. Rev. B* **85**, 134533 (2012).
- ¹⁸ G. Kresse and J. Furthmüller, *Phys. Rev. B* **54**, 11169 (1996).
- ¹⁹ J. P. Perdew, K. Burke, and M. Ernzerhof, *Phys. Rev. Lett.* **77**, 3865 (1996).
- ²⁰ F. Lu, J. Z. Zhao, and W. H. Wang, *J. Phys.: Condens. Matter* **24**, 495501 (2012).
- ²¹ V. V. Bannikov, A. L. Ivanovskii, *Physica B* **418**, 76 (2013).
- ²² We estimated the k_z values according to the free-electron final-state model, where the inner potential of 15 eV was used.
- ²³ C. Kim, F. Ronning, A. Damascelli, D. L. Feng, Z. X. Shen, B. O. Wells, Y. J. Kim, R. J. Birgeneau, M. A. Kastner, L. L. Miller, H. Eisaki, and S. Uchida, *Phys. Rev. B* **65**, 174516 (2002).
- ²⁴ H. C. Xu, M. Xu, R. Peng, Y. Zhang, Q. Q. Ge, F. Qin, M. Xia, J. J. Ying, X. H. Chen, X. L. Yu, L. J. Zou, M. Arita, K. Shimada, M. Taniguchi, D. H. Lu, B. P. Xie, and D. L. Feng, *Phys. Rev. B* **89**, 155108 (2014).
- ²⁵ D.W. Shen, B. P. Xie, J. F. Zhao, L. X. Yang, L. Fang, J. Shi, R. H. He, D. H. Lu, H. H. Wen, and D. L. Feng, *Phys. Rev. Lett.* **99**, 216404 (2007).
- ²⁶ I. I. Mazin, O. K. Andersen, O. Jepsen, O.V. Dolgov, J. Kortus, A. A. Golubov, A. B. Kuz'menko, and D. van der Marel, *Phys. Rev. Lett.* **89**, 107002 (2002).
- ²⁷ H. Uchiyama, K. M. Shen, S. Lee, A. Damascelli, D. H. Lu, D. L. Feng, Z.-X. Shen, and S. Tajima, *Phys. Rev. Lett.* **88**, 157002 (2002).